Supplemental Information (manuscript # CAN-11-1063R)

Manganese superoxide dismutase regulates a metabolic switch during the mammalian cell cycle

Ehab H. Sarsour*, Amanda L. Kalen*, Zhen Xiao[#], Timothy D. Veenstra[#], Leena Chaudhuri[$], Sujatha Venkataraman**, Philip Reigan***, Garry R. Buettner*, and Prabhat C. Goswami*

*Free Radical and Radiation Biology Division, Department of Radiation Oncology, University of Iowa, Iowa City, Iowa, USA

[#]Laboratory of Proteomics and Analytical Technologies, National Cancer Institute, Frederick, Maryland, USA

[$]Division of Hematology and Oncology, Mayo Clinic, Scottsdale, Arizona, USA

**Department of Pediatrics, University of Colorado, Denver, USA

***School of Pharmacy, University of Colorado, Denver, USA

Supplemental Information

Results presented in this section show:

(1) A minimal difference in cell cycle phase distributions in *MnSOD* (+/+), and (-/-) MEFs following re-entry into the proliferative cycle (**Table I**)

(2) An increase in MnSOD protein levels and activity in MnSOD overexpressing MB231 human mammary epithelial cancer cells (**Figure 1**)

(3) An inhibition of MnSOD activity in quiescent normal human fibroblasts was associated with an increase in glucose consumption and percent S-phase (**Figure 2**)

(4) Cell cycle phase-associated increase in cellular ROS levels was absent in *MnSOD* (-/-) MEFs (**Figure 3**)

(5) Cell cycle phase specific increase in DHE-fluorescence is primarily due to an increase in cellular steady-state levels of superoxide (**Figure 4**)

(6) Mass spectrometry results identifying lysine and arginine methylation pattern of MnSOD during quiescence and proliferation; species conservation of lysine and arginine methylation sites in MnSOD (**Figure 5**)

(7) Site directed mutagenesis approach to mutate lysine 89 and 202 of MnSOD, and engineer expression vectors of wild-type and K-to-A mutant carrying human MnSOD cDNAs **(Figure 6)**.

(8) Computer modeling of MnSOD-methylation pattern **(Figure 7)**

Materials and Methods

Cell Culture: *MnSOD* (+/+) and (-/-) MEFs were synchronized by contact inhibition followed by re-plating at a lower cell density. Cells were harvested at the time of re-plating and 24 h post-replating for flow cytometry analysis of DNA content to determine the percentage of cells in G_1-, S-, and G_2-phase.

Adenoviral infection: MB231 human mammary epithelial cancer cells were infected with 100 MOI of adenoviruses carrying a CMV-promoter driven human *MnSOD* cDNA. Cells were harvested at 72 h post-infection for analysis of MnSOD protein and activity levels.

Quiescent normal human fibroblasts were infected with 100 MOI of adenoviruses carrying a CMV-promoter driven dominant-negative form of human *MnSOD* cDNA; histidine 26 at the active site is substituted with leucine. Control and infected cells were harvested for measurements of MnSOD activity, glucose consumption rate, and percent S-phase.

Control and AdBgl II infected cells were included for comparison.

Flow cytometry measurements of MitoSOX and DHE oxdiation: Monolayer cultures were incubated with Hanks buffered salt solution (HBSS) containing 10 μM MitoSOX and flow cytometry measurements were performed using 488 nm excitation laser and 585/42 nm emission filter.

Cells in HBSS buffer were incubated with 10 μM DHE, and flow cytometry measurements of DHE-oxidation were performed using an excitation wavelength of 488 nm, and band-pass emission filters of 550/30 and 610/20 were used to distinguish between 2-OH-E^+ (superoxide) and E^+ (hydrogen peroxide).

Mean fluorescence intensity (MFI) was calculated using FlowJo software. Autofluorescence was used for background correction, and fold-change calculated relative to the MFI of G_1-cells.

Mass spectrometry: Total cellular protein extracts prepared from quiescent and proliferating cultures of normal human fibroblasts were resolved using one-dimensional gel electrophoresis. Coomassie Blue stained gel slices were excised and destained in 50% acetonitrile containing 25 mM NH_4HCO_3 (pH 8.4). Lyophilized materials were digested with 20 ng per microliter of trypsin and peptides were extracted using 70% acetonitrile containing 5% formic acid. The peptide solution was lyophilized and reconstituted in 0.1% formic acid prior to nanoflow reversed-phase liquid chromatography (nanoRPLC) tandem mass spectrometry (MS^2) analysis. NanoRPLC columns were slurry-packed with 5 μm, 300 Å pore size C-18 silica-bonded stationary reverse-phase particles (Jupiter, Phenomenex, Torrance, CA). The column was connected to an Agilent 1100 nanoLC system (Agilent Technologies, Palo Alto, CA) and coupled to a linear ion-trap (LIT) mass spectrometer operated with Xcalibur 1.4 SR1 software (LTQ, ThermoElectron, San Jose, CA). Peptides were eluted using a gradient

of mobile phase A (0.1% formic acid in water) and B (0.1% formic acid in acetonitrile) under the following conditions: 2% B at 500 nL/min in 20 min; a linear increase of 2-60% B at 250 nL/min in 100 min; 60-98% B at 250 nL/min in 10 min; and 98% B at 500 nL/min for 20 min. The LTQ was operated in a data-dependent mode in which the seven most abundant peptide molecular ions in every MS scan were sequentially selected for fragmentation and acquisition of MS^2 spectra. Tandem mass spectra were searched against the human or mouse MnSOD protein sequence using SEQUEST software (ThermoFinnigan, San Jose, CA) operating on a 40-node Beowulf cluster. Fully tryptic cleavage constraints and two missed cleavage sites were applied for search. Methylation of lysine and arginine (monomethylation: +14.0157 Da; dimethylation: +28.0313 Da) and oxidation of methionine (+15.9949 Da) residues were included as dynamic modification when searching the MS^2 spectra. The SEQUEST filtering criteria for initial identification of peptides were cross correlation (X_{corr}) scores of 1.9 for $[M + H]^{1+}$, 2.2 for $[M + 2H]^{2+}$, 3.1 for $[M + 3H]^{3+}$ ions, and a minimum delta correlation (ΔC_n) of 0.08. The MS^2 spectra of eligible peptides were manually inspected to confirm the identification of correct peptide sequence and modifications.

Site-directed mutagenesis and engineering of expression vectors containing wild-type and K-to-A mutant carrying human MnSOD cDNAs: Sal I and Not I restriction enzyme incorporated human MnSOD cDNA (669 bp) was cloned directionally into a pShooter expression vector (pCMV/cyto/myc; Invitrogen). The cloning strategy was designed to preserve the stop codon of MnSOD, while excluding the myc epitope. Insert sequence in pCMV/MnSOD was verified by sequencing.

Site-directed mutagenesis QuickChange II Kit (Stratagene) was used to mutate lysine-89 and lysine-202 of MnSOD to alanine individually and in combination. Mutagenic oligonucleotide primers for the PCR reactions were designed according to the manufacture provided protocols. pCMV/MnSOD plasmid DNAs containing K89A. K202A, and the double mutant (K89A/K202A) were further verified by sequencing.

METAFECTENE Transfection Reagent (Biontex) was used to transfect MnSOD (-/-) mouse embryonic fibroblasts, and MnSOD expression (protein levels and activity) was measured using western blotting and activity assays. Co-transfection with plasmid DNA containing GFP was included to correct for transfection efficiency.

Supplemental Table I: Flow cytometry measurements of cell cycle phase distributions in *MnSOD* (+/+) and (-/-) MEFs at the time of re-plating and 24 h post-replating.

Post replating (h)	MnSOD (+/+)			MnSOD (-/-)		
	G_1	S	G_2	G_1	S	G_2
0	82.9 ± 2.7	13.1 ± 1.8	4.0 ± 1.1	72.9 ± 1.2	15.7 ± 1.5	11.4 ± 1.2
24	49.7 ± 2.3	32.2 ± 1.0	18.1 ± 3.1	52.7 ± 2.0	29.2 ± 1.0	18.0 ± 2.3

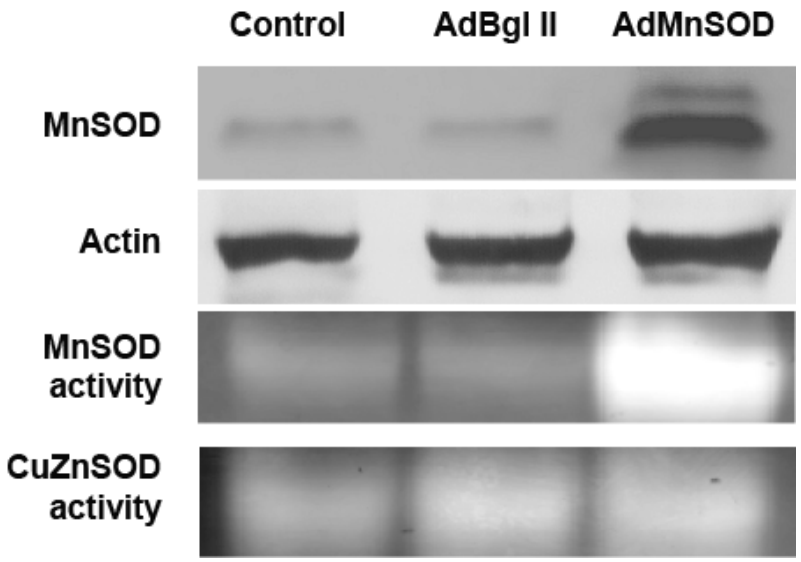

Supplemental Figure 1: MB231 cells were infected with 100 MOI of AdMnSOD, and MnSOD protein levels and activity were measured at 72 h post-infection. MnSOD protein levels and activity in control and AdBgl II infected cells were included for comparison. Actin protein levels and CuZnSOD activity were used to correct for loading.

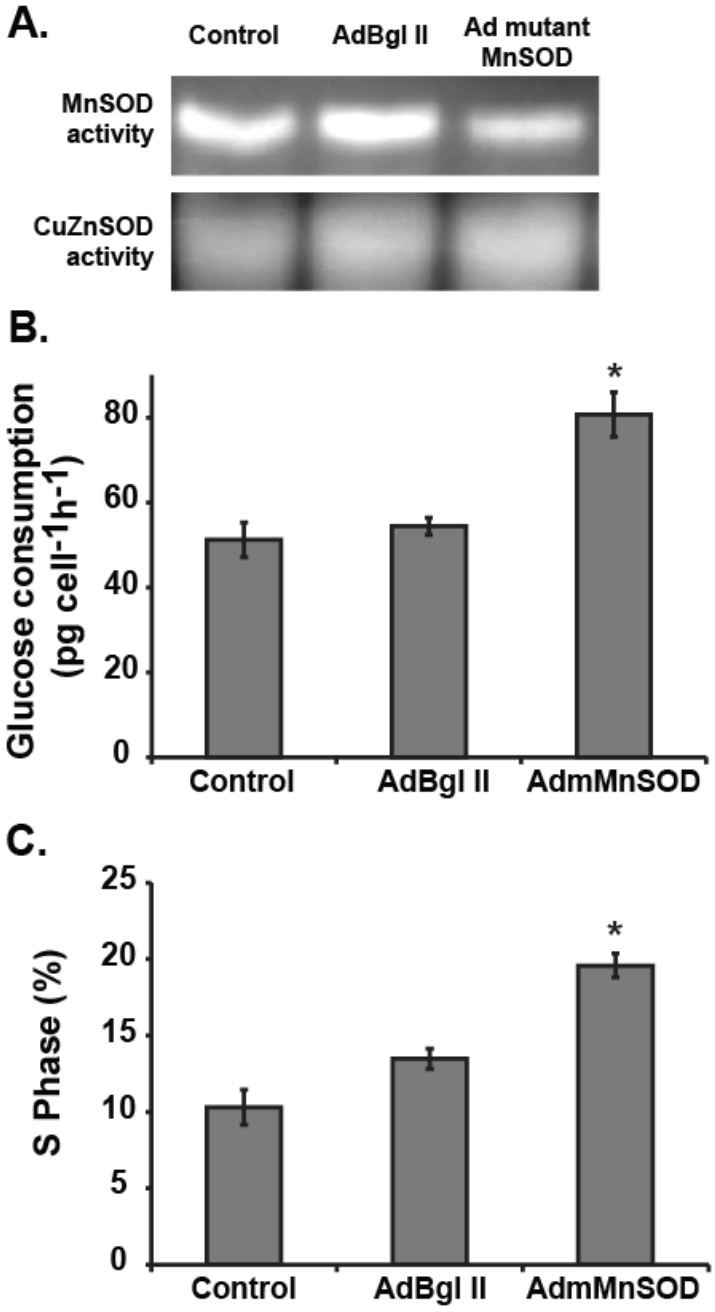

Supplemental Figure 2: Quiescent normal human fibroblasts were infected with 100 MOI adenoviruses carrying a CMV-promoter driven control (AdBgl II) and a dominant negative form of human *MnSOD* cDNA. SOD activities were measured using a gel-electrophoresis-based assay. Cells in replicate dishes were used to measure glucose consumption and percent S-phase. Asterisk indicates statistical significance relative to control and AdBgl II infected cells; $n = 3$, $P < 0.05$.

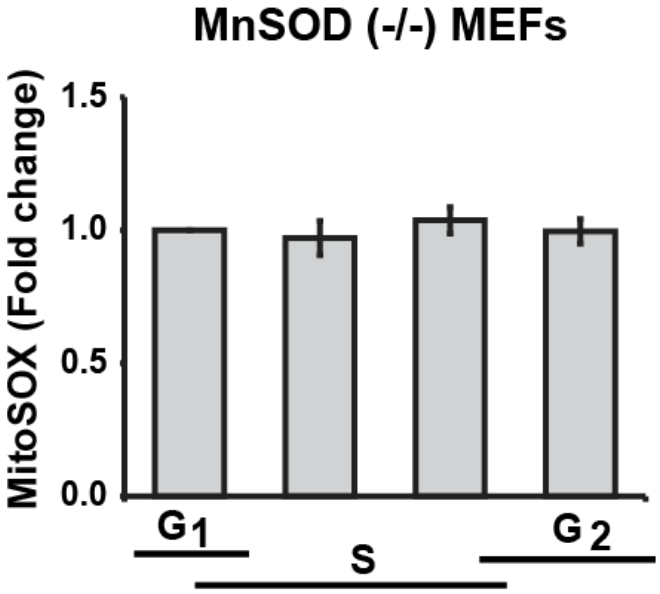

Supplemental Figure 3: Flow cytometry measurements of MitoSOX-fluorescence and DNA content in *MnSOD* (-/-) MEFs representative of G_1-, S-, and G_2-phase cells. Contact inhibited MnSOD (-/-) MEFs were replated at a lower cell density and harvested at different times post-replating for flow cytoemtry measurements of DNA content. Cells in replicate dishes were incubated with MitoSOX, and MitoSOX-oxidation was measured by flow cytometry. Fold-change was calculated relative to the MFI of G_1-cells.

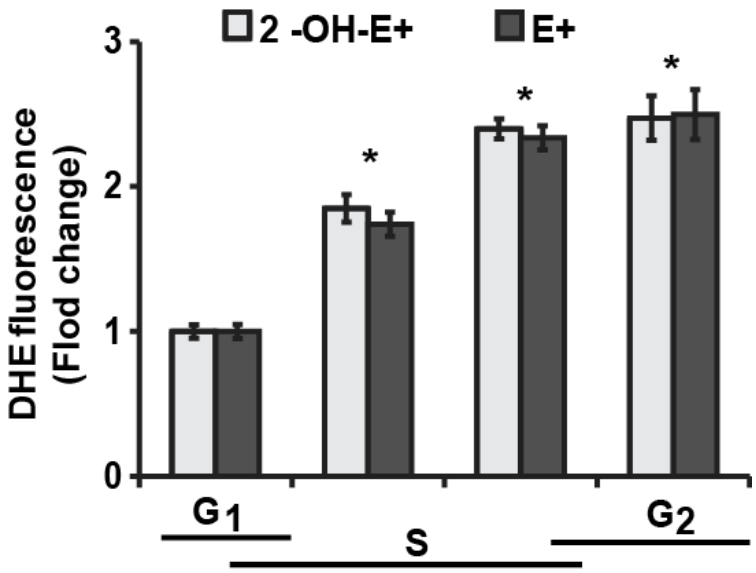

Supplemental Figure 4: Flow cytometry assay to distinguish superoxide from other oxidants. MEFs were synchronized by contact inhibition, and re-plated at a lower cell density. Cells were allowed to progress into the cell cycle and harvested at different times post-replating for flow cytometry measurements of cell cycle phase distributions. Cells in replicate dishes were incubated with DHE and DHE-oxidation was measured at an excitation wavelength of 488 nm, and band-pass emission filters of 550/30 and 610/20 were used to distinguish between 2-OH-E^+ (superoxide) and E^+ (hydrogen peroxide). Fold-change was calculated relative to the MFI of G_1-cells. Asterisk indicates statistical significance relative to the MFI of G_1-cells.

A.

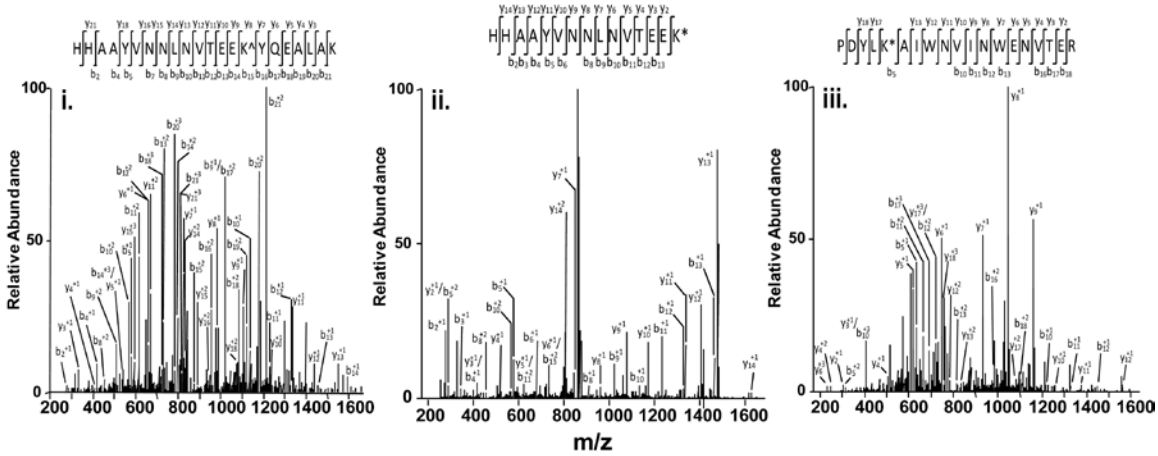

B.

	K68	K89	K122	R197 K202	R216
Human	(66) EEKYQEAL	(88) LKFNGGGH	(120) AIKRDFGS	(192) QYKNVRPDYLKAIWNVIN	(213) VTERYMAC
Chimpanzee	(43) EEKYQEAL	(65) LKFNGGGH	(97) AIKRDFGS	(169) QYKNVRPDYLKAIWNVIN	(190) VTERYMAC
Monkey	(43) EEKYQEAL	(65) LKFNGGGH	(97) AIKRDFGS	(169) QYKNVRPDYLKAIWNVIN	(190) VTERYMAC
Chicken	(68) EEKYKEAL	(90) LKFNGGGH	(122) AIKRDFGS	(194) QYKNVRPDYLKAIWNVIN	(215)VSQRYESC
Mouse	(66) EEKYHEAL	(88) LKFNGGGH	(120) AIKRDFGS	(192) QYKNVRPDYLKAIWNVIN	(213) VTERYTAC
Rat	(66) EEKYHEAL	(88) LKFNGGGH	(120) AIKRDFGS	(192) QYKNVRPDYLKAIWNVIN	(213)VSQRYIVC
Cow	(66) EEKYREAL	(88) LKFNGGGH	(120) AIKRDFGS	(192) QYKNVRPDYLKAIWNVIN	(213) VTARYTAC
Pig	(104) EEKYQEAL	(115) --------	(119) AIKRDFGS	(191) QYKNVRPDYLKAIWNVIN	(212) VTERYTAC
Dog	(66) EEKYLEAL	(89) LKFNGGGH	(121) AIKRDFGS	(193) QYKNVRPDYLKAIWNVIN	(214) VTERYMAC
Horse	(66) EEKYQEAL	(88) LKFNGGGH	(120) AIKRDFGS	(192) QYKNVRPDYLKAIWNVIN	(213) VSERYMAC
Consensus	(104) EEKYQEAL	(127) LKFNGGGH	(159) AIKRDFGS	(231) QYKNVRPDYLKAIWNVIN	(252) VTERYMAC

<u>Supplemental Figure 5</u>: (A) Total cellular protein extracts prepared from quiescent and proliferating cultures of normal human fibroblasts were resolved using gel-electrophoresis. Coomassie Blue stained gel slices were excised and subjected to tandem mass spectrometry (MS^2) analysis. Representative tandem mass spectra showing MnSOD K68 di-methylation (^, i) during quiescence and mono-methylation during proliferation (ii), while K202 (*, ii) is mono-methylated specifically during quiescence. (**B)** Conservation of the specific methylation site of lysine and arginine residues in MnSOD among species.

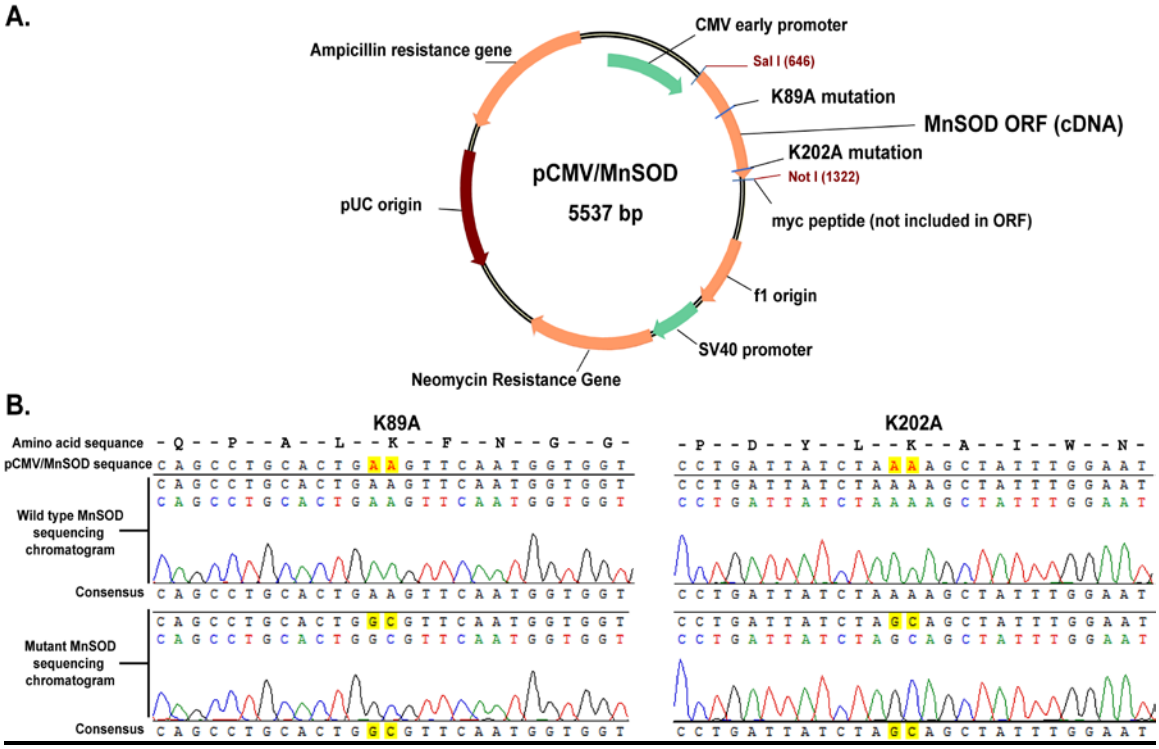

Supplemental Figure 6: (A) QuickChange II Kit (Stratagene) was used to mutate lysine 89 and lysine 202 of human MnSOD cDNA. pCMV/MnSOD plasmid DNA was engineered by cloning MnSOD wild-type and K-to-A mutant carrying human cDNAs to the multiple cloning sites of pShooter vector (Invitrogen). **(B)** Sequencing chromatograms of wild type and mutant human MnSOD cDNAs; wild type and K-to-A mutation highlighted in yellow.

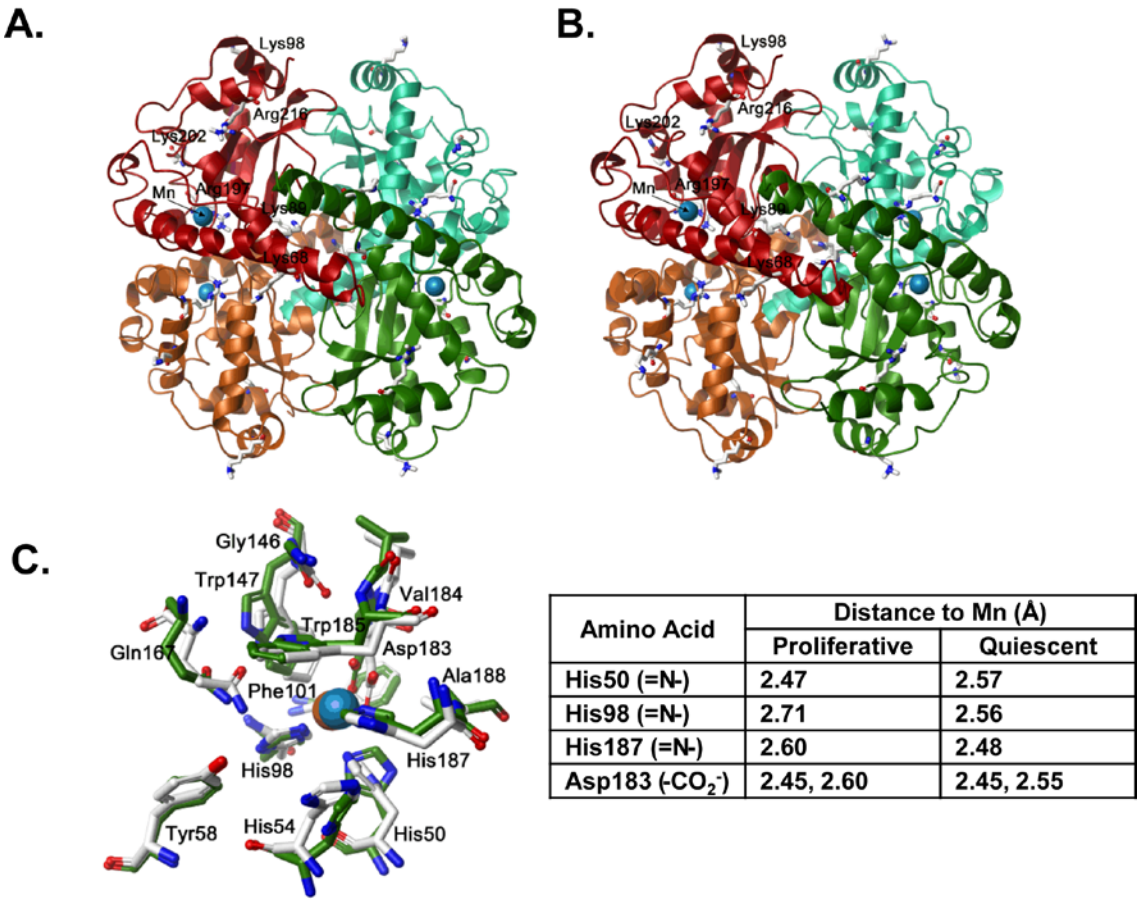

Amino Acid	Distance to Mn (Å)	
	Proliferative	Quiescent
His50 (=N-)	2.47	2.57
His98 (=N-)	2.71	2.56
His187 (=N-)	2.60	2.48
Asp183 (-CO_2^-)	2.45, 2.60	2.45, 2.55

Supplemental Figure 7: Structural and electrostatic changes in MnSOD during quiescence and proliferation. Ribbon representations of the methylated-MnSOD tetramer in proliferation and quiescence are shown **(A)** and **(B)**, respectively. The methylated residues are shown in stick display style and the manganese (Mn) ion (blue) is shown as a space fill representation. **(C)** An overlay of residues shown as stick representations in the methylated-MnSOD tetramer in proliferation (carbon atoms colored white) and in quiescence (carbon atoms colored green) within a 6Å of the Mn ion shown as a space fill representation (colored blue in the proliferative model and orange in the quiescent model). The table shows the distances (Å) of the catalytic residues H50, H98, D183, and H187 from the Mn ion in the methylated-MnSOD models.